Intermittency of Atmospheric Turbulence

L. MAHRT

Atmospheric Sciences Department, Oregon State University, Corvallis, Oregon

(Manuscript received 4 January 1988, in final form 22 July 1988)

ABSTRACT

Dimensionless structure functions such as kurtosis of the velocity gradients are computed from aircraft data for a variety of atmospheric situations in order to characterize the intermittency of the turbulence. It is necessary to distinguish between *small scale intermittency* of the velocity gradients organized by the individual main eddies and *global intermittency* associated with patchiness of turbulence on scales larger than the main eddies. Failure to make such a distinction can lead to ambiguity and inability to recognize contamination of statistics by sampling problems.

The sharp edges of the main eddies contribute to the small scale intermittency as measured by the kurtosis of the velocity gradients and other intermittency statistics. However, for some of the strongly stratified cases, global intermittency increases the kurtosis by a factor of 2 or 3 in which case the statistics reflect the global spatial variability of the turbulence (patchiness) more than the local characteristics of the turbulence itself. As a result, the kurtosis increases with record length as more of the larger scale spatial variability is incorporated. In such cases, record partitioning is employed to construct more useful estimates of the small scale intermittency.

The variation of the structure kurtosis with separation distance is normally found to obey the Kolmogorov similarity theory which has been modified to include the influence of small scale intermittency. However, the modified theory does not describe decaying turbulence nor turbulence with strong global intermittency.

The dimensionless structure function for artificial turbulence and mixtures of distributions are studied analytically. The usual dimensional structure function responds to the scale of the main building blocks (simulated eddies) while the structure kurtosis and other dimensionless moments respond to the spatial scale of the edges of the building blocks where gradients are particularly large and contribute to the tails of the frequency distribution. The dimensionless structure function of the artificial turbulence is also augmented by global intermittency posed in terms of mixtures of frequency distributions. This analytical analysis appears to explain the observed enhancement of the dimensionless structure kurtosis by the sharp edges of the main eddies and by the global intermittency of those records with strong thermal stratification.

1. Introduction

Intermittency of turbulence includes organization of small scale gradients by individual coherent eddies. With such *small scale or microscale intermittency,* dissipation of turbulence kinetic energy is confined primarily to small subregions of individual eddies. In addition, the turbulence may be patchy or *global intermittent* due to organization on scales larger than the main coherent eddies. The ambiguous term "intermittency" may refer to either small scale intermittency of dissipation or larger scale global intermittency of the main eddies.

With global intermittency, the turbulence develops as patches of eddies with large intervening areas of little turbulence activity. Episodic development of turbulence in the strongly stratified boundary layer (bursting) and associated events of downward heat flux and vertical mixing of pollutants are examples of global intermittency. Global intermittency can lead to sampling problems for computation of fluxes and other turbulence quantities (Shaw and Businger 1985; Baker and Gibson 1987).

Small scale intermittency may result from overall modulation of the turbulence by the main eddies or may occur in connection with sharp edges of the main eddies. With overall modulation, the small scale turbulence inside the eddies is sometimes larger than in the fluid outside the eddies, as often occurs with thermals (Khalsa and Businger 1977 and others). In some cases, the strongest small scale turbulence is concentrated at sharp edges of the main eddies as may occur with thermals as well as shear-driven overturning. In other observations of turbulence fields, the small scale intermittency occurs as numerous narrow zones of shear with uncertain relationship to the main coherent structures.

a. *Microfronts*

The contribution of the sharp edges of the main eddies to the intermittency of small scale turbulence can

Corresponding author address: Dr. Larry J. Mahrt, Dept. of Atmospheric Sciences, Oregon State University, Corvallis, OR 97331-2209.

occur due to generation of smaller scale turbulence by the eddy-scale shear. In Fourier space, the sharp edges of the eddies may contribute directly to higher wavenumbers and thus contribute to the variance in the inertial subrange even without generation of smaller scale eddies.

The narrow zones of concentrated shear at the edges of the main eddies are sometimes referred to as microfronts as in Kaimal and Businger (1970). Within the vagueness of the terminology, microfronts are also referred to as gust fronts, pulses, upstream edges of thermals, or in some laboratory studies simply fronts, or even "backs". In any event, the concept of the microfront provides a useful framework for organization of the study of turbulent records.

Microfronts or narrow zones of concentrated shears are often considered to be the edges of larger coherent eddies. Corrsin (1962) modeled these zones as vortex sheets. In a subsequent note, Tennekes (1968) appealed to vortex stretching to concentrate the shear across a zone as thin as the Kolmogorov microscale. In high Reynolds number turbulence, diffusion by smaller scale eddies may contribute to a broadening of the shear zone. These concentrated shear zones play an important role in the overall effect of turbulence since they are thought to be instrumental in the cascade of energy to smaller scales and appear to account for much of the total dissipation even though they occupy only a small fraction of the total volume of the turbulent fluid (Batchelor and Townsend 1949). In addition, the eddy fronts may dominate the total transport as noted by Schols (1984), Chen and Blackwelder (1978) and Kikuchi and Chiba (1985). From a practical point of view, the associated sudden changes in wind velocity can lead to cumulative structural fatigue in man-made structures such as buildings, aircraft and wind machines depending on their response functions.

Eddy microfronts in existing atmospheric data are most evident in the heated boundary layer where zones of sharp horizontal shear and convergence occur at the edge of thermals. Kaimal and Businger (1970) suggested that the sharp edges are maintained by vortex stretching induced by the vertical acceleration of the thermals. In time series of turbulence records in both stable and unstable conditions , sharp horizontal gradients or eddy microfronts appear as ramp patterns (Antonia et al. 1979; Antonia and Atkinson 1976, Schols 1984; and others) or asymmetric top hats (Mahrt 1979; Mahrt 1985; Kikuchi and Chiba 1985). Two-dimensional plan views of the velocity field in the heated boundary layer observed with doppler radar in Kropfli and Kohn (1978) and Eymard (1984) indicate considerable horizontal coherence of the shear zones suggesting that the microfronts may be vertically oriented vortex sheets.

In the study of Schols and Wartena (1986), the microfronts are associated with sharp pressure pulses. These pressure pulses may be driven by gusts of higher momentum from above. The pressure perturbation leads to vertical acceleration of warm air in significant excess of the vertical acceleration that would be expected from buoyancy alone. This rising warm air moves with weak horizontal momentum which in turn leads to horizontal convergence and sharp horizontal gradients (microfront) at the upstream edge where the stronger ambient fluid flows around the updrafts. With this point of view, surface layer thermal elements are driven more by shear than the buoyancy field. Such a viewpoint is probably most valid over a surface layer of thickness smaller than the Monin-Obukhov depth.

In a number of previous laboratory studies, similar zones of strong shear or temperature gradients have been related to the outer edges of the large eddies associated with uplifting of near-surface fluid of weak momentum, often referred to as bursting (Gibson et al. 1968; Kim et al. 1971; Laufer 1975; Willmarth 1975; Brown and Thomas 1977; Chen and Blackwelder 1978; Subramanian et al. 1982). Often the bursting is driven by transverse vortices although longitudinal modes may develop behind the microfront. Of importance is that the bursting and associated shear zones is one of the causes of the intermittent nature of mixing (Kline et al. 1967; Kim et al. 1971; Corino and Broadkey 1969; Lu and Willmarth 1973).

From a more general point of view, any vertical draft in a mean shear flow will acquire relative horizontal momentum, modified by draft entrainment and pressure effects. Horizontal convergence occurs at one edge of the draft leading to a narrow zone of sharp horizontal gradients. From another point of view, the ambient air flows around the draft inducing convergence at the upstream edge and a wake region downstream from the draft (Kovasznay et al. 1970; Chen and Blackwelder 1978; Mahrt 1981). The downstream wake region is expected to be diffuse compared to the sharp horizontal gradients maintained at the upstream microfront.

These examples would seem to apply to the concept of wind gusts which begin abruptly as sharp surges of higher wind speed as observed by a stationary observer. The composite structure of gusts constructed in Panofsky and Dutton (1984, Fig. 12.6) does indeed show a ramp structure for the horizontal velocity corresponding to a sudden increase of wind speed followed by a slower decrease of wind speed. The microfronts corresponding to the upstream edge of the thermals also appear as a gust front even though they are actually the sudden termination of low momentum air due to the passage of the upstream edge of the thermal as observed at a stationary point. The dynamic similarity between the gust front and the thermal microfront is not known.

b. Intermittency analysis

Eddies with sharp edges are somewhat ambiguous in Fourier space as was noticed by Lenschow (1970)

and shown explicitly in Schols and Wartena (1986) and Mahrt and Gamage (1987). Structures with sharp edges contribute considerable spectral and cospectral energy on scales smaller than the structures themselves. The frequency or intensity of the local shear zones does not seem to affect the rather robust occurrence of the $\frac{5}{3}$ spectral slope at small scales, at least not within the accuracy of spectra computed from geophysical records. Or conversely, the existence of a $\frac{5}{3}$ spectra slope does not imply too much about the nature of the turbulence so that velocity spectra are not particularly useful for distinguishing between different types of turbulence.

Zones of concentrated gradients and associated intermittency can be studied from a general point of view using dimensionless structure functions, such as the structure kurtosis. Although such higher moment statistics are difficult to interpret in terms of definite characteristics of the frequency distributions (Ruppert 1987) and are vulnerable to sampling problems, these statistics seem to successfully distinguish between the different types of turbulence examined in this study.

The dimensionless structure functions are examined in section 2 of this study as possible tools for studying intermittency of turbulence. The dependence of these functions on intermittent sharp gradients are studied in section 3 in terms of artificial turbulence. In sections 4–6, such functions are evaluated in terms of fast response measurements of atmospheric turbulence collected with research aircraft under a variety of atmospheric conditions.

Although this extensive aircraft data represents a large sample of high-resolution measurements of the three-dimensional fluctuating velocity field, it is limited to line measurements along the aircraft flight and three-dimensional features of the eddies cannot be examined. However, the higher moment structure functions appear to identify different types of turbulence which cannot be predicted by existing similarity theory. Dimensionless structure functions and implied intermittency are larger in newly developing turbulence or turbulence where the main eddies have sharp edges. However, in some situations global intermittency and horizontal inhomogeneity can exert a stronger influence on the values of the dimensionless structure functions.

2. Dimensionless structure functions

The structure function seems to be a direct way of statistically studying intermittency and its dependence on scale (see Anselmet et al. 1984 for a partial review). It will be seen that higher order structure functions can delineate between different types of turbulence intermittency. Although the structure functions do not allow direct comparison with existing models of turbulence based on Reynolds averaging, they avoid the somewhat arbitrary process of determining the local mean from geophysical data. The usual higher order structure function is defined as

$$D^n(r) = \langle [\phi(x + r) - \phi(x)]^n \rangle \qquad (1)$$

where ϕ is a flow variable such as temperature or one of the three velocity components, r is the separation distance between the observations and the square brackets indicate an ensemble average.

The dimensionless structure function for studying intermittency can be defined as (e.g., Frisch et al. 1978)

$$F^n(r) = D^n(r)/\{D^2(r)\}^{n/2}. \qquad (2)$$

For $n = 3$, (2) becomes the structure skewness while for $n = 4$, (2) becomes the structure kurtosis and so forth. For the usual theories of the inertial subrange, the dimensionless structure functions (2) are considerably simpler than the usual dimensional form (1). For example, the dimensionless structure function for the original Kolmogorov (1941) theory becomes independent of dissipation and separation distance r. It will been seen in later sections that intermittency including sharp local gradients and eddy microfronts can enhance the dimensionless structure function at the smaller scales. Then the dimensionless structure function decreases with separation distance.

Models of the structure function for the velocity components for the stationary inertial subrange can be argued by assuming that the downscale energy transfer across a given scale in the inertial subrange is of the scaling form

$$\epsilon(r) \sim E(r)/\tau$$

where $\epsilon(r)$ is the dissipation rate of kinetic energy averaged over the local volume of size r which is assumed to be larger than the Kolmogorov scale but small compared to the scale of the main eddies. Here $E(r)$ is the increment of specific kinetic energy associated with eddy length scale r which is cascaded to smaller scales during time scale τ. This energy transfer rate must be equal to the dissipation rate with stationary conditions (no net energy accumulated or lost at a given scale). The usual estimate of the cascading time scale is $r/v(r)$ where

$$v(r) = \{E(r)\}^{1/2}$$

then

$$\epsilon(r) \sim v(r)^3/r$$

or, in terms of an arbitrary power of the dissipation,

$$\{\epsilon(r)\}^{n/3} \sim v(r)^n/r^{n/3}.$$

Taking an ensemble average of this relationship and using the velocity structure function to estimate the ensemble average of the nth power of the velocity scale, we obtain

$$\langle \{\epsilon(r)\}^{n/3} \rangle \sim D^n(r)/r^{n/3}. \qquad (3)$$

Presumably the inertial subrange is sufficiently isotropic that $D^n(r)$ is comparable for all three velocity components. To transform this relationship into a more useful form, it is necessary to recognize that the small scale gradients and the dissipation are intermittent processes so that the ensemble average of some power of the dissipation is not equal to the power of the ensemble average as implied by the original Kolmogorov (1941) theory. Two modified approaches assume that the variation of the dissipation rate is organized by the main eddies of size L and that this variation can be approximated by a lognormal distribution of values of dissipation (Kolmogorov 1962: Yaglom 1966). Alternatively, one can approximate the dissipation as an on–off process where, at a given time, the dissipation is active only in a definite fraction of the fluid volume (Frisch et al. 1978). Either approach leads to the general form

$$\langle \{\epsilon(r)\}^{n/3} \rangle \sim \langle \epsilon \rangle^{n/3} (r/L)^{-\mu^*}$$

in which case the structure function from (3) becomes

$$D^n(r) = C_n \langle \epsilon \rangle^{n/3} r^{n/3} (r/L)^{-\mu^*} \tag{4}$$

where C_n is a nondimensional coefficient dependent on n.

For the lognormal model

$$\mu^* = (\mu/18) n(n-3)$$

where μ is a universal coefficient with a value probably between about 0.2 and 0.5 (see, for example, Anselmet et al. 1984 and papers referenced therein).

With nonzero positive $\mu^*(n)$, the second order structure function $D^2(r)$ increases faster with r compared to $\mu^* = 0$. This steepening of the slope of the dimensional structure function is apparently a result of less structure-variance at small scales due to the fact that significant small scale gradients occur only intermittently. The third order moment does not change while the higher order structure functions ($n > 3$) increase more slowly with separation distance r. The relative augmentation of the higher moment structure function at small scales probably indicates the presence of a limited number of especially strong gradients at small scales.

With the β-model (Frisch et al. 1978; Fujisaka and Mori 1979; and others),

$$\mu^* = \frac{1}{3}(3 - D)(n - 3)$$

where D is a fractal dimension describing the deformation and breakup of eddies in the inertial subrange into numerous smaller scale eddies. If the formation of the new smaller eddies occupies the entire volume of the former large eddy, then $D = 3$ in which case $\mu^* = 0$ and the $r^{2/3}$ dependence of the second order structure function is recovered. However, if the new smaller scale eddies occur only in a few subregions such as the edges of the next largest eddies where shears might be concentrated, then $D < 3$ and the structure function is modified in the same qualitative sense as with the lognormal model. D is thought to have a typical value of 2.5 (see Frisch et al. 1978 and references therein). In the present study, we will compare the predictions of the lognormal and β-models with aircraft observations. We cannot directly test the underlying assumptions and will therefore consider the models as empirical relationships.

For the models with format (4), the dimensionless structure function (2) assumes the simple form

$$F^n(r) = Cr^{[(n/2)\mu^*(2) - \mu^*(n)]} \tag{5}$$

where C is a function of n and L.

For the lognormal model, the dimensionless structure function (5) becomes

$$F^n(r) = Cr^{-(\mu n/18)(n-2)} \tag{6}$$

while for the β-model, the dimensionless structure function (5) (Frisch et al. 1978) becomes

$$F^n(r) = Cr^{-(1/2)(3-D)(n-2)}. \tag{7}$$

Since the dimensionless structure function is independent of the dissipation, it is simpler to evaluate than the dimensional form (4).

The above results apply only for separation distances which are small compared to the scale of the main coherent eddies and large compared to the Kolmogorov scale and therefore are valid only for scales in the inertial subrange. For this range of scales, the predicted dimensionless structure functions (6–7) are independent of separation distance for the original Kolmogorov theory without modification for intermittency ($\mu = 0$, $D = 3$). With modification due to small scale intermittency ($\mu > 0$, $D < 3$), the dimensionless structure function decreases with separation distance. The larger values at small separation distances can probably be associated with the tails of the frequency distribution for the velocity gradients associated with occasional especially large gradients. In the next section, we will study the influence of sharp edges of idealized large eddies on the dimensionless structure function.

3. Artificial turbulence

In this section, we will examine the influence of building blocks of artificial turbulence on the behavior of the structure function. Such simplified analyses are necessary because the higher moment structure functions by themselves do not provide unambiguous information about the frequency distributions of the time series (e.g., Ruppert 1987). The goal of this section is therefore not to be particularly realistic but rather to understand how the structure function responds to the geometry of simple structures.

More specifically, we are interested in the direct contribution of the concentrated shear at the edges of the main eddies to the small scale variance in the in-

ertial subrange. In the usual framework of the inertial subrange in Fourier space, the contribution of the sharp edges of the main eddies would be misinterpreted as distinct smaller scale turbulence. In fact, power law theories of the dependence of the structure function on separation distance in the inertial subrange of scales are usually argued in terms of a cascade of energy to smaller and smaller scales usually attributed to sequential instabilities.

In contrast, Pierrehumbert and Widnall (1982) and others have argued that the energy cascade in the inertial subrange of actual turbulent flows can be limited to few scales of motion resulting from only a few sequential instabilities. The continuous dependence on scale would then presumably result from wavenumber smearing of a given scale of motion. In fact, power law dependencies of the structure function even occur with simple time series consisting only of identical structures of one scale and amplitude (Van Atta 1977).

Here we will study the structure function of artificial time series consisting of idealized structures with sharp edges which contribute directly to the structure function at small separation distances. Toward this goal it will be useful to express the structure function in the form

$$D^n(r) = \int f[\Delta\phi(r)][\Delta\phi(r)]^n df \qquad (8)$$

where

$$[\Delta\phi(r)]^n = [\phi(x+r) - \phi(x)]^n$$

and f is the relative frequency of a given value $\Delta\phi$. In the following examples of artificial records with simple building blocks, (8) will be applied as a discrete summation.

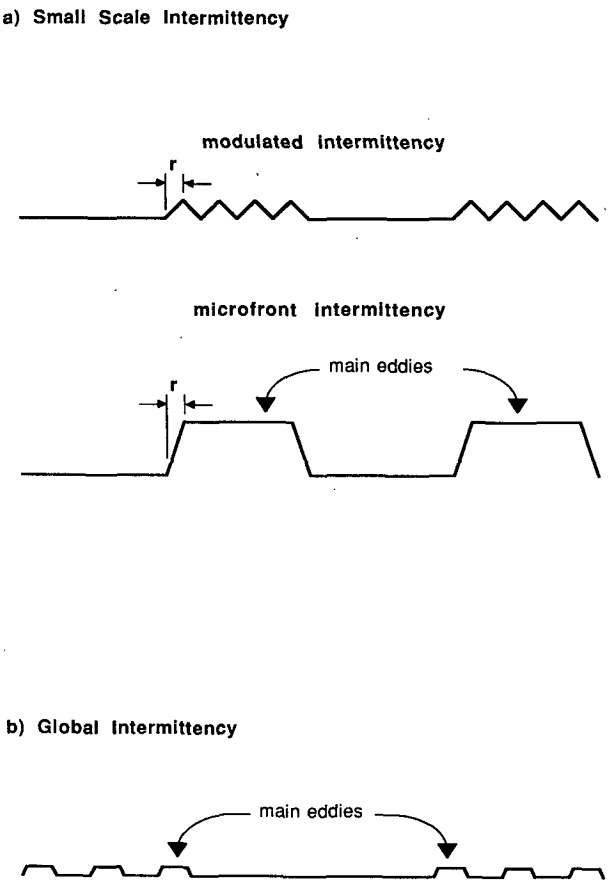

FIG. 1. Artificial examples of (a) small scale intermittency and (b) global intermittency. With idealized modulated intermittency, $p \to \infty$ corresponding to (11). With microfront intermittency, $f^* \to$ small, corresponding to (12).

a. Two-mode structure

The simplest possible class of artificial records consists of only two different magnitudes of $(\Delta\phi)^2$. For simplicity, we will not explicitly consider the dependence on separation distance until the next subsection. Consider the case where $(\Delta\phi)^2$ assumes only one of two values; for example, the larger value $(\Delta\phi_2{}^2)$ could crudely simulate the effect of sharp edges of the main eddies while a smaller value $(\Delta\phi_1{}^2)$ simulates background turbulence. Figure 1a shows two examples of artificial discrete records which lead to two-mode distributions with $\Delta\phi_1 = 0$ when the separation width r is the minimum resolution and moves one point (distance r) at a time.

The corresponding even order structure function (8) for the two-mode case consists of only two terms

$$D^n = f_1(\Delta\phi_1{}^2)^{n/2} + f_2(\Delta\phi_2{}^2)^{n/2}$$
$$= f_1(\Delta\phi_1{}^2)^{n/2}(1 + f^* p^{n/2}) \qquad (9)$$

where f_1 and f_2 are the relative fractions of the record occupied by magnitude $\Delta\phi_1{}^2$ and $\Delta\phi_2{}^2$, respectively, f^* is the ratio of the two relative frequencies

$$f^* = f_2/f_1$$

while p is the ratio of squares of the two magnitudes

$$p = \Delta\phi_2{}^2/\Delta\phi_1{}^2.$$

For the two-mode artificial turbulence (9), the dimensionless structure (2) becomes

$$F^n(r) = f_1{}^{-(1/2)(n-2)}(1 + f^* p^{n/2})/(1 + f^* p)^{(n/2)}. \qquad (10)$$

Note that with only one mode ($p = 1$), the dimensionless structure function is unity. If both modes occur with equal frequency ($f^* = 1$), but the second mode is much stronger ($p \gg 1$), the dimensionless structure function (10) becomes approximately

$$F^n = 2^{(1/2)(n-2)} \qquad (11)$$

and thus decreases with n.

For the case where the stronger mode is relatively rare ($f^* \ll 1$) but $f^* p$ remains large compared to unity, the dimensionless structure function becomes

$$F^n = f_2{}^{-(1/2)(n-2)} \tag{12}$$

In this case, the dimensionless structure function increases more rapidly with n compared to (11) since $f_2 \ll 1$. Thus, both the difference of the strength between the two modes and the difference between the relative frequencies of the two modes enhance the nondimensional structure function. This conclusion is predicted by (10) for the entire range of values of p and f^*.

Two simple examples of artificial two-mode records are noted in Fig. 1a. In the first case, the stronger fluctuations occur for 50% of the record and crudely simulate the case where the small scale turbulence is modulated by the larger scale eddies (modulated small scale intermittency). The dimensionless structure function is modest for this case. In the second example, the strong fluctuations are limited to the edges of the main artificial eddies (microfront small scale intermittency). Since the microfront gradients are particularly large and occupy only a small fraction of the record, the dimensionless structure function is large.

The above example reenforces our expectation that rare strong events augment the values of the higher moment structure function although it does not prove the converse that observed large values of the dimensionless structure function imply the existence of rare strong events. The above example also shows that the infrequency and relative amplitude of the events jointly enhance the values of the higher moment structure function in a nonlinear way (10). In the next subsection, the analysis is expanded to include the dependence on separation distance.

b. *Regularly spaced top hat functions*

We now consider dependence on horizontal scale for an artificial record consisting of regularly spaced "top hat" or square pulse functions of width L bordered by transition zones of width αL (Fig. 2a). This is one of the simplest artificial records that allows explicit study of the dependence of the structure function on the separation distance r. This artificial record crudely approximates the conceptual picture of coherent structures where gradients are weak in the interior and concentrated at the edges. That is, the intermittency of the record is organized by the main eddies. Top hat functions have been used to approximate the structure of thermals and plumes and appear to be useful in the absence of significant vertical wind shear where the main eddies are likely to be symmetric with respect to horizontal distance.

To generalize the results of this subsection, we scale r and L by the interval distance between observations so that r becomes the number of data intervals in the separation window, L is the width of the flat regions

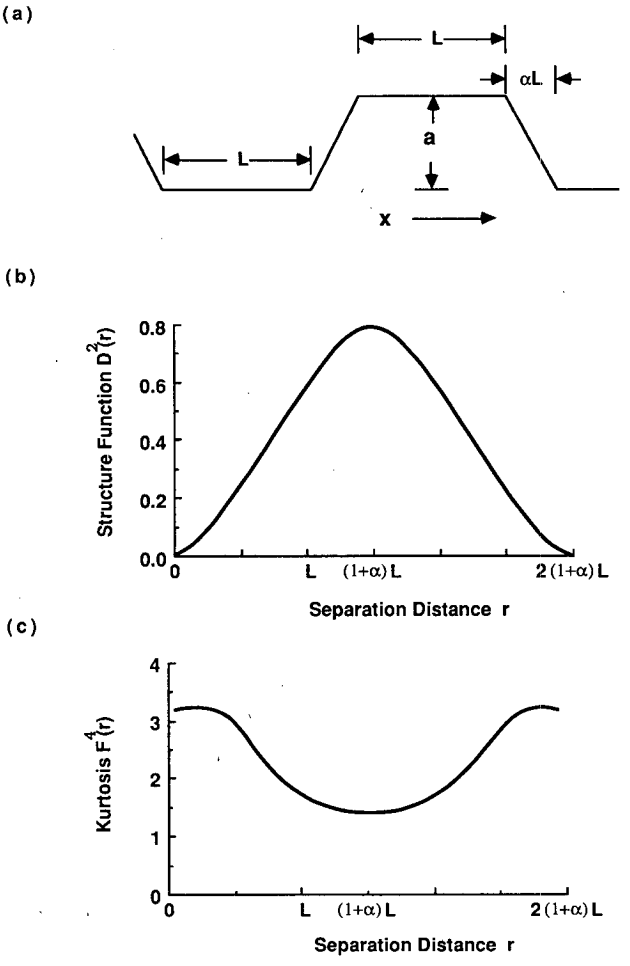

FIG. 2. (a) Top hat structure with transition zones, (b) second-order structure function for a time series of such top hat structures and (c) the corresponding kurtosis.

of the top hats expressed in number of data intervals and αL is the width of the transition zones expressed in number of data intervals. To compute the structure function, the separation window moves through the discretized record one data interval at a time and generates a time series of $\Delta\phi(x) = \phi(x + r) - \phi(x)$. This time series is periodic in x with a wavelength of $2L(1 + \alpha)$ so that computation of the structure function requires summing over only one wavelength.

If the separation window is less than or equal to the width of the transitions zones, we obtain the following distribution of values of $\Delta\phi$ for each transition zone where ϕ increases with x

straddle terms

$$N(a/\alpha L) = 2$$
$$N(2a/\alpha L) = 2$$
$$\cdots$$
$$N((r-1)/\alpha L) = 2 \tag{13a}$$

transition-embedded term

$$N(r/\alpha L) = \alpha L + 1 - r$$

where N is the number of observations of a given value of $\Delta\phi$. The frequency distribution is symmetric with respect to $\Delta\phi = 0$ in that the same distribution occurs for negative values of $\Delta\phi$ in the complementary transition zone where ϕ decreases with x. Straddle terms are those where the separation "window" used to calculate $\Delta\phi$ straddles one of the edges of the transition zone while the transition-embedded term corresponds to the samples where the separation window is entirely within the transition zone.

To complete the distribution for one cycle, we must include the remaining samples where the separation window is embedded within a flat region of zero gradient. In particular

$$N(\Delta\phi = 0) = L + 1 - r \tag{13b}$$

for each of the two flat sections of a top hat cycle. Note that if $\alpha L = 1$, so that the width of the transition zone is one data interval, then $(\Delta\phi)^2$ is either zero or a^2 as in the two-mode example of the previous subsection.

The relative frequencies are computed by dividing the number of observations N (13) by the total number of data intervals in one cycle $2L(1 + \alpha)$. Then, the nth order structure function (8) becomes

$$D^n(r) = [2L(\alpha + 1)]^{-1}\left\{2\sum_{j=1}^{r-1}\left[\left(\frac{ja}{\alpha L}\right)^n + \left(-\frac{ja}{\alpha L}\right)^n\right] + (\alpha L + 1 - r)\left[\left(\frac{ra}{\alpha L}\right)^n + \left(-\frac{ra}{\alpha L}\right)^n\right]\right\}. \tag{14}$$

The summed terms in (14) are due to the $4(r - 1)$ straddle terms where $\Delta\phi$ is proportional to the fractional overlap $j/\alpha L$ of the separation window with the transition zone. The remaining term not involving summation is the contribution from the cases where the separation interval is embedded entirely within the transition zone corresponding to the last term in (13a).

(i) *Small separation distance ($r \ll \alpha L$)*

For this case, only the embedded term (unsummed term) in (14) is important and the even ordered structure function becomes approximately

$$D^n(r) = \alpha\,(ra/\alpha L)^n. \tag{15}$$

Thus for small r, the structure function increases as the nth power of the separation distance. The structure function $D^2(r)$ increases as r^2 which is steeper than the unmodified Kolmogorov prediction of the inertial subrange of $r^{2/3}$. However, the artificial time series can be generalized to include random spacing and amplitude in such a manner to produce the $r^{2/3}$ dependence analogous to the analysis of Van Atta (1978).

The even order dimensionless structure function (2) corresponding to (15) becomes

$$F^n(r) = [\alpha]^{-(1/2)(n-2)} \tag{16}$$

where we have made use of the condition that the width of the transition zone is significantly narrower than the interior flat region of the top hat ($\alpha \ll 1$).

The dimensionless structure function for this case is again simpler than the dimensional one and is independent of both the separation distance and amplitude. As in the two-mode example, the dimensionless structure function increases with the order n. In this example (16), the dimensionless structure function also increases with the sharpness of the edges (smallness of α). As α decreases, the transition zones occupy a smaller fraction of the record increasing the intermittency. In other words, the dimensionless structure function for small separation distances serves as an index for the intensity of the microfront transitions and related intermittency of the small scale gradients.

(ii) *Separation distance approaches the width of the transition zone*

Then the structure function is dominated by the first bracketed term in (14) corresponding to cases where the separation window straddles one of the edges of the transition zone. The even order structure function is then approximately,

$$D^n(r) = [2/L(1 + \alpha)]\sum_{j}^{r-1}(ja/\alpha L)^n$$

or for narrow transition zones (small α), approximately

$$D^n(r) = (2/L)(a/\alpha L)^n\sum_{j}^{r-1}(j)^n. \tag{17}$$

Therefore as long as the transition width is large compared to the data interval, the structure function (17) for $r \gg 1$ varies as r^n, to the lowest order of approximation.

The corresponding dimensionless structure function is

$$F^n(r) = \left(\frac{2}{L}\right)^{-(1/2)(n-2)}\frac{\sum_{j}^{r-1} j^n}{[\sum_{j}^{r-1} j^2]^{n/2}} \tag{18}$$

which becomes independent of r to the lowest order of approximation.

Therefore as the separation distance approaches the width of the transition zone, the structure function and dimensionless structure function (Fig. 1) still depend on the separation distance in a manner qualitatively similar to the dependence on separation distance for values small compared to the transition width (15)–(16).

(iii) *Separation distance is greater than the width of the transition zones but smaller than the width of the top hats*

Then the structure function is of the form

$$D^n(r) = [2L(\alpha + 1)]^{-1}\left\{2\sum_{j=1}^{\alpha L-1}\left[\left(\frac{ja}{\alpha L}\right)^n + \left(-\frac{ja}{\alpha L}\right)^n\right] + (r - \alpha L + 1)[a^n + (-a)^n]\right\}. \quad (19)$$

The first term involving the summation results from cases where the separation window straddles the boundary of the transition zone leading to a partial overlap distance of $j/\alpha L$. The second term results from the cases where the transition zone is now embedded within the separation window in contrast to (14) where the smaller separation window was embedded within the transition zone.

(iv) *Separation distance is just slightly larger than the width of the transition zones*

Then the overlap term in (19) dominates and the dependence on the separation distance and amplitude of the top hats is not too different from the case where the separation distance is slightly less than the transition width (17).

(v) *Separation distance much larger than the width of the transition zones but still smaller than the width of the top hat*

Then the embedded term [second term in Eq. (19)] dominates and the even order structure function is approximately

$$D^n(r) = (r/L)a^n \quad (20)$$

and the structure function increases only linearly with the separation distance r which is weaker than the r^n dependence for smaller separation distances (15). The dimensionless structure function corresponding to (20) is simply

$$F^n(r) = (r/L)^{-(1/2)(n-2)} \quad (21)$$

and thus decreases with increasing separation distance. This decrease becomes rapid for the higher order functions.

Of importance is that the dimensionless structure function is approximately independent of the separation distance until the separation distance reaches values comparable to the transition width (Fig. 2c) and then decreases with larger values of the separation distance. *Therefore the separation distance at which the dimensionless structure function begins to decrease with increasing separation distance is a measure of the widths of the transition zones* at least for the above class of artificial records. One might therefore expect that in actual turbulence data, the dimensionless structure function would be an index for typical widths of the local regions of intensified gradients.

(vi) *Separation distance exceeds one half of the wavelength of the top hat function*

When the separation distance exceeds the width of the top hat plus the width of one transition zone, the structure function begins to decrease (Fig. 2b) due to interference between two adjacent transition zones simultaneously captured in the separation window. The dimensionless structure function continues to decrease with increasing separation distance. As the separation distance approaches $2L(1 + \alpha)$, the wavelength of the top hat pattern, the structure function approaches zero while the dimensionless structure function approaches a nonzero minimum. *Thus the structure function reaches a maximum at a separation distance approximately equal to the width of the top hats.* Note that when the separation distance is exactly $2L(1 + \alpha)$, the dimensionless structure function in the discrete case becomes undefined as both the numerator and denomenator vanish.

Numerical evaluation of more complicated artificial time series, where the amplitude and spacing between the top hats include a random component of variation, indicates that the dimensionless structure function is still related to the width of the transitions. The main difference is that the dimensionless structure function begins to decrease with separation distance at scales somewhat smaller than the width of the transitions zones.

In summary, for the simple artificial record above, the maximum of the dimensional structure function is related to the width of the main structures while the maximum of the dimensionless structure function indicates the widths of the transition zones of the main eddies. That is the dimensionless structure functions are more influenced by the extreme values at the tails of the frequency distributions of the gradients.

c. *Ramp functions*

The simplest artificial record which contains asymmetry of the main structures is one of regularly spaced ramp functions (Van Atta 1977). Ramp functions, consisting of a linear increase with x followed by a discontinuous drop to the original value, appear to roughly approximate the main eddies in many turbulent flows with shear-induced asymmetry (Antonia et al. 1979, 1982).

For ramp functions where the width of the linear increase is l, separated by distance s of zero gradient, the dimensionless structure function for separation distances which are small compared to $l + s$ but large compared to the Kolmogorov scale, is of the form

$$F^n(r) = [r/(l + s)]^{-(1/2)(n-2)}.$$

This relationship follows from (2.12) in Van Atta (1977) or (2) in Antonia et al. (1982). Here the dimensionless structure function decreases with increasing separation distance for all values of the separation

distance. This is because the transition zones of the ramp functions have zero thickness and therefore cannot be resolved. However, the increase of the structure function with the order n is of the same form as in previous examples.

d. Global intermittency

The previous subsections indicate that the dimensionless structure function can identify the scale of the strongest gradients for simple records. However, geophysical records are also complicated by global intermittency of the main eddies and inhomogeneity on larger scales. To study the potential influence of global intermittency on higher moment statistics of geophysical turbulence, consider an idealized record consisting of two modes, each with its own frequency distribution of gradients. Johnson and Kotz (1970) have shown that two mixtures of normal distributions with equal means but different variances lead to a mixture kurtosis greater than those of the two individual distributions. We will consider the case where distributions are non-Gaussian as occurs with distributions of velocity gradients in actual turbulence. One mode will represent patches of strong turbulence which occupies a small fraction of the record $f_2 \ll 1$ and is characterized by large velocity differences $\delta u(r)$ with estimated variance $E[(\delta u)^2]$ and a mode of weaker background turbulence which occupies a large fraction of the record ($f_1 = 1 - f_2$) and is characterized by small velocity differences $\delta v(r)$ with variance $E[(\delta v)^2] \ll E[(\delta u)^2]$.

Both distributions of gradients are assumed to have zero mean. The structure moment (8) is then just the weighted average of the expected values of the structure moments for the two individual distributions. The nth order structure moment for the sum of the two distributions leads to the following estimate of the dimensionless structure function (2) for the mixture of the two distributions

$$F^n(r) = [f_2 E(\delta u^n) + f_1 E(\delta v^n)]/ [f_2 E(\delta u^2) + f_1 E(\delta v^2)]^{n/2}. \quad (22)$$

The kurtosis of the entire record can be expressed in terms of the kurtosis of each of the two distributions by dividing (22) into two terms and factoring out the appropriate variance from the denominator for each term. Then we obtain

$$F^n(r) = f_2 F^n(r, \delta u)/[f_2 + s f_1]^{n/2} + f_1 F^n(r, \delta v)/[f_1 + (f_2/s)]^{n/2} \quad (23)$$

where:

$$F^n(r, u) = E(\delta u^n)/E(\delta u^2)^{n/2}$$
$$F^n(r, v) = E(\delta v^n)/E(\delta v^2)^{n/2}$$
$$s = E(\delta v^2)/[E(\delta u^2)] \ll 1.$$

Of interest is that the dimensionless structure function of the entire "record" of the mixture of distributions $F^n(r)$ can be greater than that for both of the two types of distributions comprising the record. For example, consider the case where both distributions are characterized by the same dimensionless structure function

$$F^n(r, \delta u) = F^n(r, \delta v),$$

then

$$[F^n(r)/F^n(r, \delta u)] = [f_2 + s^{n/2} f_1]/[f_2 + s f_1]^{n/2}. \quad (24)$$

The dimensionless structure function of the entire record is greater than that of both of the individual distributions if the numerator on the right-hand side is greater than the denominator. For the kurtosis ($n = 4$), this condition is satisfied if

$$s(2 - s) < 1. \quad (25)$$

This condition is satisfied for all $s < 1$ so that the kurtosis of the mixture is always greater than the kurtosis values for the individual distributions. Relatively speaking, the variance is more influenced by the prevalent weaker gradients δv while the higher moments [numerator of (22)] are more influenced by the less common stronger gradients δu.

In other terms, the inhomogeneity of this simple record enhances the kurtosis beyond the values for the subrecords. Conversely the kurtosis of the entire record reflects the inhomogeneity of the record in addition to the characteristics of the turbulence within the different parts of the record. Since the turbulence in most geophysical records is characterized by at least some inhomogeneity, care must be exercised when interpreting the higher moment statistics. An analysis of the meaning of the kurtosis of velocity gradients in records of atmospheric turbulence will be conducted in sections 5 and 6.

4. Atmospheric cases

This section and subsequent sections indicate that dimensionless structure functions are useful tools for distinguishing between different types of atmospheric turbulence. In particular, turbulence which is just developing or is maintained only intermittently is characterized by large values of the dimensionless structure function while more continuous turbulence is characterized by smaller values.

Here we will analyze a variety of different types of turbulence as observed by research aircraft with fast response instrumentation. Aircraft data will be analyzed in the bora over the northern coastal range of Yugoslavia (Smith 1987) collected during the Alpine Experiment (ALPEX). We have organized the ALPEX records into four classes: 1) very weak globally intermittent turbulence far upstream from the mountain

TABLE 1. Characteristics for individual flight legs include the buoyancy length for $r = 10$ m [Eq. (26)], the structure function for vertical velocity D^2 (10 m), kurtosis for vertical velocity $F4$ (10 m) and slope of the structure function [Eq. (27)] between 10 and 50 m. For ALPEX legs, the height above ground is omitted since surface terrain is mountainous. The turbulence in HAPEX and in the lower boundary layer in PHOENIX are characterized by upward heat flux; the other legs are characterized by weak or downward heat flux. Class "average" values are simple unweighted averages of values for all of the legs in the class while "composited" values are computed by combining the legs of a given class into one time series.

Program-class	Leg	Height (m, AGL)	Length (km)	Buoyancy length ($r \sim 10$ m)	Structure function ($r \sim 10$ m)	Kurtosis ($r \sim 10$ m)	Slope (10–50 m)
				SESAME			
5 May							
strongly stratified	1	70	27	1	0.003	5.1	−0.15
	2	90	13	2	0.009	6.7	−0.11
	3	70	17	2	0.013	12.5	−0.18
	4	55	16	2	0.008	7.1	−0.18
	5	20	19	<1	0.002	13.7	−0.35
Average						9.0	−0.20
Composited						14.7	−0.28
6 May—windy	1	20	15	16	0.10	4.0	−0.02
	2	14	12	51	0.20	4.3	−0.12
	3	35	12	56	0.26	4.6	−0.17
	4	165	13	38	0.27	5.0	−0.22
	5	35	15	39	0.25	4.3	−0.14
Average						4.4	−0.14
Composited						5.4	−0.11
				ALPEX			
6 March							
Far upstream, Weak	v0		69	10	0.011	16.2	−0.11
	w0		83	5	0.004	11.0	0.19
	y4		130	4	0.005	12.8	0.38
	z3		133	2	0.002	13.3	−0.12
Average						13.3	0.08
Composited						18.9	0.09
Near ridge	v1		37	18	0.03	16.3	0.06
	w1		31	40	0.15	22.8	−0.20
	x2		25	42	0.07	27.6	−0.31
Average						22.3	−0.15
Composited						32.2	−0.14
Downstream, strong	v2		43	208	0.95	6.2	−0.06
	v3		23	48	0.12	7.0	−0.21
	w2		28	169	0.75	8.8	−0.18
	w3		35	78	0.25	9.6	−0.40
	x3		26	65	0.18	11.6	−0.22
	x4		21	25	0.05	11.8	−0.10
	y2		67	50	0.10	5.7	−0.17
	z2		11	53	0.07	8.0	−0.09
Average						8.6	−0.18
Composited						14.1	−0.06
Far downstream, weak	z1		94	14	0.01	8.9	0.03
	x5		22	6	0.01	9.1	0.42
	w4		89	13	0.02	8.0	0.03
Average						8.7	0.16
Composited						9.4	0.06
				PHOENIX			
17 June 1984							
Lower boundary layer	9	165	21	118	0.32	7.1	−0.25
	10	158	23	118	0.22	5.8	−0.15
	19	159	24	119	0.27	5.4	−0.12

TABLE 1. (*Continued*)

Program-class	Leg	Height (m, AGL)	Length (km)	Buoyancy length ($r \sim 10$ m)	Structure function ($r \sim 10$ m)	Kurtosis ($r \sim 10$ m)	Slope (10–50 m)
	20	162	23	112	0.26	4.7	−0.03
	29	165	24	103	0.24	5.9	−0.26
	30	163	20	91	0.22	5.1	−0.10
Average						5.7	−0.15
Composited						5.9	−0.16
Upper boundary layer	3	1738	26	50	0.03	8.3	−0.27
	4	1746	26	40	0.03	7.9	−0.11
	13	2059	22	79	0.10	6.6	−0.17
	14	2070	24	90	0.14	8.2	−0.15
	23	2221	24	79	0.08	8.9	−0.25
	24	2243	24	84	0.07	16.3	−0.22
Average						9.4	−0.20
Composited						11.4	−0.18
22 June 1984							
Lower boundary layer	9	163	25	115	0.30	5.5	−0.17
	10	151	22	108	0.27	6.3	−0.17
	19	165	24	164	0.27	5.8	−0.16
	20	162	22	154	0.29	4.9	−0.14
Average						5.6	−0.16
Composited						5.6	−0.16
Upper boundary layer	3	3060	22	168	0.16	11.4	−0.09
	4	3068	24	128	0.11	7.6	−0.11
	13	3564	19	190	0.23	8.9	−0.18
	14	3579	23	193	0.23	5.9	−0.14
Average						8.6	−0.13
Composited						8.8	−0.12
				HAPEX			
19 May 86	1	150	120	90	0.34	6.0	−0.12
	2	150	120	97	0.40	5.7	−0.18
	3	150	120	93	0.41	5.3	−0.10
	4	150	120	90	0.39	5.5	−0.22
	5	150	120	105	0.49	5.3	−0.18
	6	150	80	119	0.50	5.3	−0.20
Average						5.5	−0.17
Composited						5.6	−0.17
25 May 86	1	150	120	95	0.31	5.9	−0.18
	2	150	120	102	0.38	5.7	−0.15
	3	150	120	125	0.36	5.7	−0.16
	4	150	120	120	0.37	5.8	−0.15
	5	150	120	125	0.37	6.0	−0.17
	6	150		129	0.38	5.7	−0.12
Average						5.8	−0.15
Composited						5.8	−0.16

range, 2) developing globally intermittent turbulence above the mountain range, 3) strong turbulence immediately downstream from the mountain range and 4) weaker turbulence farther downstream which is also globally intermittent (Table 1).

Aircraft data from the heated convective boundary layer will be analyzed from the Hydrological and Atmospheric Pilot Experiment (HAPEX) described by André (1988). Six legs, 120 km long and approximately 100 m above the surface, are analyzed for each of two fair weather days. These legs were flown over a large pine forest in Southwest France and represent some of the longest records of boundary-layer turbulence. Statistics between the six legs are remarkably similar (Table 1) due to the large sample size and due to approximate stationarity and relative homogeneity. Aircraft

data will also be analyzed in a weakly heated boundary layer observed during the PHOENIX experiment. Here the influence of heating is constrained by the influence of warm air advection aloft and the mean shear assumes some importance. Aircraft legs were repeatedly flown at five different levels in the boundary layer on each of two days, a total of thirty legs on the first day and twenty legs on the second day. For each day, the legs are collected into two classes, one near the surface and one near the top.

Finally aircraft data will be analyzed from the nocturnal stable periods during the Severe Environmental and Mesoscale Experiment (SESAME). This data includes both windy conditions with weak stratification and nearly calm conditions with strong stratification (Mahrt and Gamage 1987). On the first day, five legs are analyzed at the top of a strongly stratified surface inversion layer, about 50 m deep.[1] Intermittent turbulence is driven by modest shear at the top of the inversion layer while the strong stratification inhibits any significant turbulence within the inversion layer itself. On the second day, winds nearly 20 m s^{-1} maintain a boundary layer of 300 m depth in spite of strong surface radiative heat loss.

5. Structure kurtosis

In the present analysis, we will examine the structure function for the horizontal gradients of vertical motion. The horizontal velocity components are more contaminated by larger scale motions while in strongly stratified flow, small scale temperature gradients may survive at locations where the turbulence is no longer active. In general, the nondimensional structure function for temperature was greater than that for vertical momentum as might be expected from the simulations of Kerr (1985). We will analyze even order moments. Odd order moments are generated primarily by mean vertical wind shear but will not be explicitly considered in this study.

Increasing the order of the moment primarily amplifies features in the dependence of the structure function on horizontal scale apparently due to increased emphasis on the most sharply defined structures. This enhances the differences between different records but also aggrevates sampling problems which appear to be important in some of the atmospheric records. However, the qualitative interpretation offered below does not depend crucially on the order of the moment. In this section, we will study the fourth-order moments (kurtosis) at a small separation distance of 10 m in order to emphasize small scale gradients. The separation distance of 10 m appears to be the smallest scale free of the influence of the instrument response time scale and process filtering. The analysis was also carried out with 50 m separation distance; although the kurtosis values were generally smaller, the variations between types of turbulence were qualitatively similar to the results with 10 m separation distance and will not be reported here. Presumably even larger values of the kurtosis could be found if the processed data resolution had been finer than 10 m. The dependence of the structure function on horizontal scale will be explicitly studied in section 5.

We now briefly examine the influence of the large variation of stability between records on the structure kurtosis. Structure functions in the surface layer exhibit a systematic dependence on stability (Wyngaard et al. 1971; Fairall and Larsen 1986). Here we will use the structure buoyancy length (Mahrt and Gamage 1987) as a local stability parameter since it was less affected by sampling problems and the computational procedure is more straightforward compared to computation of a flux-based local stability length. The structure buoyancy length is defined as

$$d(r) = D_w^2(r)/\{(g/\Theta)[D_\theta^2(r)]^{1/2}\} \qquad (26)$$

where the subscripts w and θ indicate the structure functions for vertical velocity and potential temperature, respectively, g is the acceleration of gravity and Θ is a basic state potential temperature. The structure buoyancy length possesses the additional advantage that it systematically increases with separation distance up to typically 100 m where it becomes nearly independent of horizontal scale. However the structure buoyancy length is always positive and one must sometimes consult the correlation between potential temperature and vertical motion in order to distinguish between stable and unstable cases. Table 1 lists the structure buoyancy length for approximately 10 m separation distance which are typically a factor of three smaller than the asymptotic values approached for separation distances greater than 100 m.

The records with the largest values of the kurtosis occur with strong stability (small buoyancy length); however, the scatter is large and the link between stratification and dimensionless structure functions will be found to be rather indirect. Other factors are, at least collectively, more important. The kurtosis is smallest in turbulence which is more or less continuous (not globally intermittent) and relatively homogeneous. For example, the kurtosis at 10 m separation distance averages only 4.4 for the windy SESAME class (Table 1). The kurtosis increases modestly to about 5.5 for the low level legs in the heated boundary layers during HAPEX and PHOENIX where the sharp edges of thermals are often characterized by large concentrated gradients of vertical velocity. The larger kurtosis and

[1] A sixth leg was omitted since it contained an anomalously strong updraft coincident with very warm surface radiation temperatures. This feature was apparently associated with a man-made structure. In this case, the unusually large kurtosis for this leg served as an indicator of an anomalously large event. An unusually large value of the dimensionless structure function for one of the legs in the PHOENIX data also flagged a 100 m section with bogus vertical motion data.

intermittency is also due to greater intensity of fluctuating gradients inside the thermals compared to the regions between thermals.

Most of the remaining records are characterized by global intermittency associated with strong stratification or characterized by other larger scale inhomogeneity of the turbulence. Both effects greatly enhance the kurtosis values. Recall that records containing mixtures of different turbulence strengths corresponding to different distributions of velocity gradients may have kurtosis values larger than those values for the different distributions contributing to the record (section 3). Due to such effects, kurtosis values are typically on the order of ten in the globally intermittent turbulence in the strongly stratified SESAME flow, the inhomogeneous turbulence in the upper part of the PHOENIX boundary layer and the globally intermittent turbulence in the bora flow (ALPEX) far downstream from the mountain range and also upstream from the mountain range.

Kurtosis values are extremely large, exceeding twenty, in the developing globally intermittent turbulence above the mountain range. Here the developing patches of turbulence are intense leading to larger contrast with the intervening regions of little turbulence. This large contrast augments the kurtosis values. The sharp edges of the drafts in the turbulence patches lead to a smaller enhancement of the kurtosis.

We tentatively conclude that global intermittency significantly increases the kurtosis and other higher moments to the extent that values of the dimensionless structure function represents the variation of the turbulence more than the nature of the turbulence itself. Analogous complications have been noted in the study of variance/mean ratios describing spatial variations of vegetation (Pielou 1969).

We attempt to isolate the enhancement of kurtosis due to global intermittency by dividing the records into subrecords corresponding to patches of turbulence and intervening regions of weaker or nonexistent turbulence. For the developing turbulence above the mountain range, the kurtosis within the patches of significant turbulence and within the intervening regions of weak or no turbulence is a factor of two or more smaller than the kurtosis value for the entire record.

The reduction of kurtosis is not as large when the records are partitioned into equal subrecords since such arbitrary partitions may sometimes include both turbulent and nonturbulent flow within a given subrecord. From a more general point of view, the kurtosis and other higher moments show a general increase with record length (Fig. 3) for a variety of reasons. In the trivial limit of the shortest possible record with only one computed velocity gradient, the kurtosis is unity. As the record length increases, the kurtosis increases due to turbulent fluctuations including the influence of small scale intermittency organized by the main eddies. As the record length becomes long enough to include a sample of the main eddies, the kurtosis value may become nearly independent of the record length. This occurs in the thermally driven HAPEX and low level PHOENIX turbulence and in the continuous turbulence of the windy SESAME case (Fig. 3). The kurtosis shows little increase as the record length increases beyond 5 km suggesting that the influence of inhomogeneity is minimal. In fact the kurtosis values for different record lengths in the HAPEX and low level PHOENIX cases reach the same value of approximately 5.6.

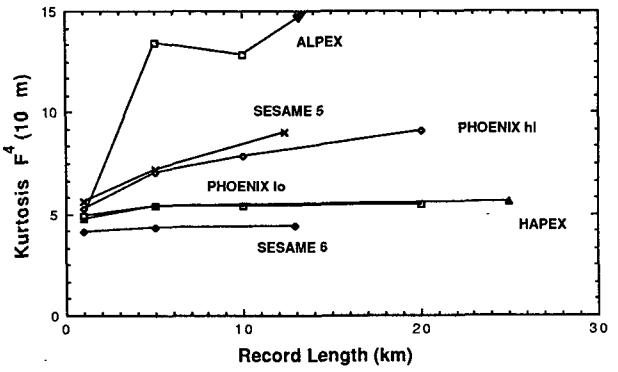

FIG. 3. Averaged values of the kurtosis as a function of the subrecord length; subrecords are created by equal partitioning of the entire record. To facilitate comparison between cases, records were partitioned into 1 km, 5 km, 10 km and when possible 20 km segments. The HAPEX and low level PHOENIX lines coincide. The significant difference between the SESAME 6 values compared to the PHOENIX low-level and HAPEX values is somewhat dwarfed in this particular figure by the large influence of global intermittency on the other cases.

In the turbulence with global intermittency or other significant inhomogeneity, the kurtosis continues to increase as the record length increases beyond 5 km and more of the inhomogeneity is captured (Fig. 3). This sensitivity to record length implies that the statistical characteristics of the turbulence itself can not be quantitatively established in these cases without further analysis such as record partitioning. Note that the kurtosis values for both the homogeneous cases and the globally intermittent and inhomogeneous cases show much less variation when the subrecord lengths are too short to include the influence of global intermittency and inhomogeneity.

To form even larger records, values of Δw from individual records of a given class were combined to form one large sample. The kurtosis of the entire sample is then computed by simply summing the structure variance and fourth order moments using all of the data from all of the individual records and then substituting directly into (2). The final kurtosis value is not influenced by the boundaries of individual records since the separation window (of width r) is never allowed to straddle the boundaries of individual records. The resulting kurtosis for the inhomogeneous classes (composited kurtosis, Table 1) are typically 50% larger than

the values for the individual records within the class probably due to variations of turbulence strength between records. Such differences are small in the more homogeneous cases of HAPEX and low-level PHOENIX turbulence.

The above subdivision of records and combining of records reveals that the dimensionless structure functions will increase with record length due to small scale intermittency, global intermittency and general inhomogeneity of the turbulence. This result was predicted by the theoretical analysis of mixtures of distributions in section 3. The augmentation of the dimensionless structure functions by the patchiness of the turbulence underscores the need to distinguish between different types of intermittency when studying geophysical turbulence records. Furthermore the kurtosis and other higher moments of a given turbulence field cannot be represented by a single value. In the more homogeneous records with continuous turbulence, the kurtosis becomes almost independent of record length once the record length becomes a factor of ten larger than the scale of the main eddies. For globally intermittent turbulence, the value of the kurtosis is more representative of the spatial variation of the turbulence than the turbulence itself, at least without partitioning the record.

From another point of view, increasing the record size to bolster the sample size of the main eddies increases the impact of the inhomogeneity of the turbulence. In cases of obvious global intermittency, the degree of small scale intermittency intrinsic to the turbulence itself can be estimated by computing statistics for many short records. Then values of the dimensionless structure function can be averaged subject to the usual problems of averaging ratios.

6. Dependence on scale

The structure functions for the atmospheric aircraft data usually increase with horizontal scale (separation distance) according to a power law dependence (see section 2) at least for scales which are small compared to the size of the main eddies. The higher order dimensionless structure function usually decreases with separation distance as predicted (section 2). In this section we wish to explore the usefulness of the modified Kolmogorov theories for describing this scale dependence. We will also attempt to determine the causes of the occasional breakdown of the power law dependence. We can anticipate that global intermittency and the sensitivity of the slope of the structure functions to sampling problems are important in some of the records.

Here we estimate the exponents of the power law dependence on separation distance (5) as

$$f(n) \equiv \partial \ln F^n(r)/\partial \ln(r)$$
$$= [\ln F^n(r_2) - \ln F^n(r_1)]/[\ln(r_2) - \ln(r_1)]. \quad (27)$$

With the lognormal model (6) and β-model (7), $F^n(r)$ can be written in the form

$$F^n(r) = C(L, n)r^{\zeta(n)}.$$

Then

$$f(n) = \zeta(n)$$

where $\zeta(n) = -(\mu n/18)(n - 2)$ for the lognormal model and $\zeta(n) = -\frac{1}{2}(3 - D)(n - 2)$ for the β-model.

For the atmospheric cases, a power law dependence for the dimensional structure function (constant slope in logarithmic coordinates) was generally satisfied at least for separation distances between 10 and 50 m which will be the assigned values for r_1 and r_2, respectively. In cases of relatively strong turbulence, the power law dependence on separation distance extended to scales larger than 100 m. Table 1 lists the values of the slope $f(n)$ for the various records.

The observed slope of the dimensionless structure function is typically negative due to the enhancement of the dimensionless structure function at small separation distances by small scale intermittency. This small scale enhancement is predicted by the modified theories of the dimensionless structure function for the inertial subrange presented in section 2 and the analysis of artificial turbulence in section 3.

Values of the slope of the kurtosis of vertical velocity gradients for the more homogeneous data sets are generally near -0.16 (Table 1). The scatter of the slope values is large in globally intermittent turbulence. The estimation of the slope is more vulnerable to sampling problems than the dimensionless structure function itself. For weak turbulence, the slope is actually positive (Table 1) indicating a lack of intense small scale gradients. Much of this turbulence may be in a state of decay where any sharp small scale gradients have been smoothed by small scale diffusion.

For kurtosis, the "lognormal model" (see section 2) predicts slopes between -0.09 ($\mu = 0.2$) and -0.22 ($\mu = 0.5$). For the observed values of the slopes, $\mu = 0.3$ or 0.4 would be a reasonable approximation for the lognormal model. For the β-model, the recommended fractal dimension of 2.5 (section 2) produces slopes which are too steep for the present data; a fractal dimension of 2.85 fits the data better. This statistical fitting does not necessarily imply that the physical assumptions underlying these models are valid.

In some cases, the dimensionless structure function does not begin to decrease with increasing separation distance until the separation distance exceeds a few tens of meters leading to near-zero values or even positive values of the slopes at small separation distances. The idealized analysis of section 3 indicates that the dimensionless structure function does not begin to decrease until the separation distance is comparable to the width of the transition zones at the edges of the

main coherent structures. Closer investigation of the special observed cases indicate that a few vigorous structures with sharp edges are sometimes responsible this behavior. It is not known if such examples represent sampling problems and that negative slopes would be established at small scales with longer records.

Most of the positive values of the slope $f(n)$ occur for records with weak turbulence much of which appears to be decaying. The positive slope values are probably due to weak small scale gradients due to diffusive smoothing which dominates in decaying turbulence and selective viscous dissipation of the smallest scales.

7. Conclusions

The study of intermittency requires the conceptual distinction between larger scale *global intermittency* where the turbulence eddies occur in patches and the always present *small scale intermittency* where the spatial variation of the fine scale velocity gradients and dissipation are organized by individual main turbulent eddies. In other terms, global intermittency occurs on scales larger than the scale of the main turbulent eddies while small scale intermittency of dissipation occurs on scales comparable to, or smaller than, the main turbulent eddies. The strongest small scale velocity gradients are often concentrated at the edges of the main eddies or microfronts corresponding to significant small scale intermittency. The above partitioning between global and small scale intermittency fails to account for the simultaneous variation on a variety of scales but serves to relieve some of the existing conceptual ambiguity of "intermittency" and its measurement.

The dimensionless structure function is particularly useful for distinguishing between intermittency behavior in different types of atmospheric flows. Such differences are difficult to isolate using spectra or the usual dimensional structure function. In the present study, the analysis has concentrated on the kurtosis of horizontal gradients of vertical velocity although the following conclusions also qualitatively apply to other variables and other even-ordered moments. The kurtosis was evaluated from fast response aircraft data collected under a variety of atmospheric conditions during four different field programs.

The kurtosis and small scale intermittency of the small scale velocity gradients is about 25% larger in turbulence in heated boundary layers as compared to turbulence in windy near neutral boundary layers. Apparently the small-scale intermittency is modestly augmented by the rather sharp edges of the thermals. The stronger velocity gradients at the edges of the main eddies contribute to the tails of the frequency distributions of the velocity gradients and thus increases the values of higher moment functions.

However, the largest kurtosis occurs in globally intermittent turbulence where the turbulence occurs only in patches due to the constraint of the stable stratification. In this case, large values of the kurtosis and other dimensionless higher moment functions are more indicative of the spatial variation of the turbulence than the nature of the turbulence itself within the individual patches. In these cases, the interpretation of any higher moment statistics is ambiguous without further analysis such as partitioning the record. For example, the kurtosis of individual patches of turbulence were much smaller than values for the entire record and more comparable to values for continuous turbulence without global intermittency. Therefore, the influence of small scale intermittency can be partially isolated by breaking the record into subrecords and averaging the statistics computed for the individual subrecords.

Because of this influence of global intermittency or other larger scale inhomogeneity, the kurtosis increases with increasing record length until the main impact of the spatial variation is captured. In contrast, for records with continuous turbulence and only weak spatial inhomogeneity, the kurtosis becomes independent of the record length when the record length becomes an order of magnitude larger than the main turbulent eddies.

The enhancement of dimensionless structure functions by both the sharp edges of the main structures and by global intermittency is predicted by the analytical analysis of artificial turbulence and analysis of mixtures of distributions carried out in section 3. The analysis of the mixture of two distributions indicates that the kurtosis and other higher moments for the entire mixture are greater than the higher moments for either of the individual distributions, thus reflecting important enhancement of kurtosis by the inhomogeneity of the sample.

The analysis of artificial turbulence also indicates that the dimensional structure function responds to the scale of the main eddies while dimensionless structure functions such as kurtosis respond to the widths of the transition zones at the edges of the eddies; that is, the dimensionless structure functions responds more to the largest velocity gradients at the tails of the frequency distribution. The magnitude of the dimensionless structure function for the artificial turbulence is approximately independent of separation distance at scales smaller than the transitions and then decrease with increasing separation distance at larger scales. This behavior did occur for some of the aircraft records. However for most of the atmospheric records, the structure kurtosis decreases with separation distance beginning at the smallest resolvable scales, probably due to a variety of transition widths and variety of other activity in complex turbulence flows.

The slope of the general decrease of the dimensionless structure function with separation distance occurring for most of the records is roughly approximated

by the lognormal modification of the Kolmogorov similarity theory with the usual values for μ and could be statistically approximated by the β-model with a fractal dimension of about 2.85. For records with weak decaying turbulence, the dimensionless structure function actually increases with separation distance due to lack of intense small scale gradients and thus behaves quite differently from the similarity prediction.

Global intermittency also complicates the estimation of fluxes in that a small fraction of the record of inadequate sample size may dominate the total flux. Fluxes and other turbulence quantities can assume meaning only after completing an analysis of dependence on scale, record length (Wyngaard 1971; Lenschow and Stankov 1986) and sampling problems analogous to the calculations carried out in section 5. However, the analogy to the intermittency of the dimensionless structure function is not complete since the influence of global intermittency is partly a problem of computing ratios while the calculation of fluxes and other quantities based on deviations from a local mean and must contend with any sensitivity to the definition of the local mean.

Acknowledgments. The useful comments of Nimal Gamage, Rick Katz, Ed Waymire and the anonymous reviewers are greatly appreciated as is the computational work of Wayne Gibson and technical assistance of Paul Ruscher. This material is based upon work supported by the Meteorology, Experimental Meteorology and Global Atmospheric Programs of the National Science Foundation under Grants ATM-8521349, ATM-8512535 and ATM-8518461. The National Center for Atmospheric Research is acknowledged for computer resources and the use of the Queen Air research aircraft in SESAME, the Electra in ALPEX and the King Air in HAPEX.

REFERENCES

André, J. C., 1988: Evaporation over land-surfaces: First results from HAPEX-MOBILHY special observing period. *Ann. Géophys.*, **6**, 477–492.

Anselmet, F., Y. Gagne, E. J. Hopfinger and R. A. Antonia, 1984: High-order velocity structure functions in turbulent shear flows. *J. Fluid Mech.*, **140**, 63–89.

Antonia, R. A., and J. D. Atkinson, 1976: A ramp model for turbulent temperature fluctuations. *Phys. Fluids*, **19**, 1273–1278.

——, A. J. Chambers, C. A. Friehe and C. W. Van Atta, 1979: Temperature ramps in the atmospheric surface layer. *J. Atmos. Sci.*, **36**, 99–108.

——, —— and E. F. Bradley, 1982: Relationships between structure functions and temperature ramps in the atmospheric surface layer. *Bound.-Layer Meteor.*, **23**, 395–403.

Baker, M. A., and C. H. Gibson, 1987: Sampling turbulence in the stratified ocean: statistical consequences of strong intermittency. *J. Phys. Oceanogr.*, **17**, 1817–1836.

Batchelor, G. K., and A. A. Townsend, 1949: The nature of turbulent motion at large wave-numbers. *Proc. Roy. Soc. London*, **A199**, 238–255.

Brown, G. L., and S. W. Thomas, 1977: Large structure in a turbulent boundary layer. *Phys. Fluids*, **20**(Suppl.), 243–252.

Chen, C. H. P., and R. F. Blackwelder, 1978: Large-scale motion in turbulent boundary layer: A study using temperature contamination. *J. Fluid Mech.*, **89**, 1–31.

Corino, E. R., and R. S. Brodkey, 1969: A visual investigation of the wall region in turbulent flow. *J. Fluid Mech.*, **37**, 1–30.

Corrsin, S., 1962: Turbulent dissipation fluctuations. *Phys. Fluids*, **5**, 1301–1302.

Eymard, L., 1984: Radar analysis of a tropical convective boundary layer with shallow cumulus clouds. *J. Atmos. Sci.*, **41**, 1380–1393.

Fairall, C. W., and S. E. Larsen, 1986: Inertial-dissipation methods and turbulence fluxes at the air–ocean interface. *Bound.-Layer Meteor.*, **34**, 287–301.

Frisch, U., P. L. Sulem and M. Nelkin, 1978: A simple dynamical model of intermittent fully developed turbulence. *J. Fluid Mech.*, **87**, 719–736.

Fujisaka, H., and H. Mori, 1979: A maximum principle for determining the intermittency exponent u of fully developed steady turbulence. *Prog. Theor. Phys.*, **62**, 54–60.

Gibson, C. H., C. C. Chen and S. C. Lin, 1968: Measurements of turbulent velocity and temperature fluctuations in the wake of a sphere. *AIAA J.*, **6**, 642–649.

Johnson, N. L., and S. Kotz, 1970: *Continuous Univariate Distributions–1*. Houghton Mifflin, Vol. 1, 87–92.

Kaimal, J. C., and J. A. Businger, 1970: Case studies of a convective plume and a dust devil. *J. Appl. Meteor.*, **9**, 612–620.

Kerr, R. M., 1985: Higher-order derivative correlations and the alignment of small-scale structures in isotropic numerical turbulence. *J. Fluid Mech.*, **153**, 31–58.

Khalsa, S. J. S., and J. A. Businger, 1977: The drag coefficient as determined by the dissipation method and its relation to intermittent convection in the surface layer. *Bound.-Layer Meteor.*, **12**, 273–297.

Kikuchi T., and O. Chiba, 1985: Step like temperature fluctuations associated with inverted ramps in a stable surface layer *Bound.-Layer Meteor.* **31**, 51–63.

Kim, H. T., S. J. Kline and W. C. Reynolds, 1971: The production of turbulence near a smooth wall in a turbulent boundary layer. *J. Fluid Mech.*, **50**, 133–160.

Kline, S. J., W. C. Reynolds, F. A. Schraub and P. W. Runstadler, 1967: The structure of turbulent boundary layers. *J. Fluid Mech.*, **30**, 741–774.

Kolmogorov, A. N., 1941: The local structure of turbulence in an incompressible fluid for very large Reynolds numbers. *Dokl. Akad. Nauk. S.S.S.R.*, **30**, 301–305.

——, 1962: A refinement of previous hypotheses concerning the local structure of turbulence in a viscous incompressible fluid at high Reynolds number. *J. Fluid Mech.*, **13**, 82–85.

Kovasznay, L. S. G., V. Kibens and R. F. Blackwelder, 1970: Large-scale motion in the intermittent region of a turbulent boundary layer. *J. Fluid Mech.*, **41**, 283–325.

Kropfli, R. A., and N. M. Kohn, 1978: Persistent horizontal rolls in the urban mixed layer as revealed by dual-Doppler radar. *J. Appl. Meteor.*, **17**, 669–676.

Laufer, J., 1975: New trends in experimental turbulence research. *Annual Rev. Fluid Mech.*, **7**, 307–326.

Lenschow, D. H., 1970: Airplane measurements of planetary boundary layer structure. *J. Appl. Meteor.*, **9**, 874–884.

——, and B. B. Stankov, 1986: Length scales in the convective boundary layer. *J. Atmos. Sci.*, **43**, 1198–1209.

Lu, S. S., and W. W. Willmarth, 1973: Measurements of the structure of the Reynolds stress in a turbulent boundary layer. *J. Fluid Mech.*, **60**, 481–511.

Mahrt, L., 1979: Penetrative convection at the top of a growing boundary layer. *Quart. J. Roy. Meteor. Soc.*, **105**, 469–485.

——, 1981: Circulations in a sheared inversion layer at the mixed layer top. *J. Meteor. Soc. Japan*, **59**, 238–241.

——, 1985: Vertical structure and turbulence in the very stable boundary layer. *J. Atmos. Sci.*, **42**, 2333–2349.

——, and N. Gamage, 1987: Observations of turbulence in stratified flow. *J. Atmos. Sci.*, **44**, 1106–1121.

Panofsky, H. A., and J. A. Dutton, 1984: *Atmospheric Turbulence*. Wiley and Sons, 397 pp.

Pielou, E. C., 1969: *An Introduction to Mathematical Ecology*. Wiley, 100–102.

Pierrehumbert, R. T., and S. E. Widnall, 1982: The two and three-dimensional instabilities of a spatially periodic shear layer. *J. Fluid Mech.*, **114**, 59–82.

Ruppert, D., 1987: What is kurtosis? An influence approach. *Amer. Stat.*, **41**, 1–5.

Schols, J. L. J., 1984: The detection and measurement of turbulent structures in the atmospheric surface layer. *Bound.-Layer Meteor.*, **29**, 39–58.

——, and L. Wartena, 1986: A dynamical description of turbulent structures in the near neutral atmospheric surface layer: The role of static pressure fluctuations. *Bound.-Layer Meteor.*, **34**, 1–15.

Shaw, W. J., and J. A. Businger, 1985: Intermittency and the organization of turbulence in the near-neutral marine atmospheric boundary layer. *J. Atmos. Sci.*, **42**, 2563–2584.

Smith, R. B., 1987: Aerial observations of the Yugoslavian Bora. *J. Atmos. Sci.*, **44**, 269–297.

Subramanian, C. S., S. Rajagopalan, R. A. Antonia and A. J. Chambers, 1982: Comparison of conditional sampling and averaging techniques in a turbulent boundary layer. *J. Fluid Mech.*, **123**, 335–362.

Tennekes, H., 1968: Simple model for the small-scale structure of turbulence. *Phys. Fluids*, **11**, 669–671.

Van Atta, C. W., 1977: Effect of coherent structures on structure functions of temperature in the atmospheric boundary layer. *Arch. Mech.*, **29**, 161–171.

——, 1978: Structure and mechanisms of turbulence II. *Lecture Notes in Physics*, H. Fiedler, Ed., Springer-Verlag, p. 76.

Willmarth, W. W., 1975: Structure of turbulence in boundary layers. *Adv. Appl. Mech.*, **15**, 159–254.

Wyngaard, J. C., 1973: On surface layer turbulence. Workshop on Micrometeorology. D. A. Haugen, Ed., Amer Meteor. Soc.

——, Y. Izumi and S. A. Collins, 1971: Behavior of the refractive index structure parameter near the ground. *J. Opt. Soc. Am.*, **61**, 1646–1650.

Yaglom, A. M., 1966: The influence of fluctuations in energy dissipation on the shape of turbulence characteristics in the inertial interval. *Sov. Phys. Dokl.*, **11**, 26–29.